VOL. 18, NO. 14, JULY 2023 ISSN 1819-6608
ARPN Journal of Engineering and Applied Sciences

www.arpnjournals.com

MECHANICAL PROPERTIES OF 17-4 PH STEEL MANUFACTURED BY POWDER BED FUSION

María Vargas[1], Felix Christian[2], Rafael Bolivar[1] and Luz Hernández[1]
[1]Pamplona University, Km Via B/manga, Pamplona, Colombia
[2]Engineering and Industrial Development Center (CIDESI), Av. Playa, Av. Pie de la Cuesta, Desarrollo San Pablo, Santiago de Querétaro, Qro., México
E-Mail: rbolivarl@unipamplona.edu.co

ABSTRACT

The mechanical properties, such as the modulus of elasticity, yield strength, and ultimate tensile strength, were validated to precipitate-hardened 17-4PH stainless steel fabricated by the laser powder bed fusion process. Initially, six specimens were manufactured by varying the thickness and the fabrication angle, followed by tensile testing to obtain the modulus and yield strength. The results showed that the mechanical properties were low; therefore, further research is needed to change the manufacturing parameters to improve the mechanical properties.

Keywords: additive manufacturing; mechanical properties 17-4PH; powder bed fusion.

Manuscript Received 22 May 2023; Revised 19 September 2023; Published 30 September 2023

1. INTRODUCTION

The current manufacturing industry has had to confront changing people's needs, seeking a customer-centric approach. New manufacturing technologies can address this problem; however, their implementation is costly because it requires several changes and high computational resources, but this does not mean they cannot be implemented. The use of digital technologies contributes to the solution of advanced processes and continuous production in the industry, allowing coordinated control for the reduction of failures, loss of time, and improvement of product quality [1].

Since 1960, Advanced Manufacturing Technologies (AMT) have been studied, moving from digital circuits and systems to programmable logic controllers (PLCs) and computer numerical control (CNC) machine tools. This was the starting point for the third industrial revolution. Before 1960, AMT developed and implemented automation in artisanal workshops, turning them into automatic production lines, thus helping companies produce low-cost mass products. As a result, AMT is used in companies to improve competitiveness [2]. For example, Germany is the most competitive country in the world in the manufacturing industry due to its actual production of machines, having the advantage of being a leader in the research and development of new technologies, following a structured approach to take advantage of the benefits of AMT.

Therefore, Additive Manufacturing (AM) is a versatile and innovative alternative with experience at all levels. However, some problems associated with this technology are the high cost of implementing the process, the few available materials, and, most importantly, the high demand for resources to study and optimize process parameters [3]. Laser-based Additive Manufacturing (LAM) is advancing rapidly and has been well-received in industries such as biomedical and aerospace, but the repeatability and quality of the manufactured parts make this process difficult to spread. LAM manufactures layer-by-layer pieces from a computer-aided design (CAD), using a laser to melt the material and generate a liquid pool to produce the layer [4].

Powder Bed Fusion (LPBF), also commonly known as Selective Laser Melting (SLM), is one of the AM processes that uses a focused laser beam to selectively melt a bed of metallic powder to build three-dimensional components layer by layer. This process creates highly complex parts with different shapes and mechanical properties better than the forging technique. Therefore, it has become the preferred process for manufacturing molds with previously challenging cooling channels by conventional processes [5].

The material used in the research was 17-4PH, which is a precipitation-hardened stainless steel. It has good mechanical strength, corrosion resistance, machinability, and toughness. Due to its precipitated hardened product from a martensitic matrix is used for chemical, electrical, maritime, and aerospace applications for its maximum service temperature of 315°C [6].

Currently, many works focus on the design of experiments to achieve a desirable microstructure, but this method takes a lot of time and money. In contrast, a computational method is more efficient, where the cooling rate is controlled to achieve control of the microstructure.

Cooling rate and temperature gradient are metal solidification's most important physical phenomena, establishing the grain's orientation, size, and morphology. The cooling rate in component manufacturing is one of the most critical factors. For example, if it is high, it could cause high material segregations, resulting in low layer hardness and, therefore, a high cooling rate produces finer grains [4].

On the contrary, commercial 17-4 PH stainless steel possesses a martensitic structure that differs from the 17-4 PH stainless steel used in additive manufacturing (AM). Although specific studies have identified a prevalent martensitic structure, a minor presence of retained austenite (RA) has been observed when

fabricating it within an argon (Ar) atmosphere [5]. Conversely, a combination of martensite and austenite is achieved using a nitrogen (N2) atmosphere. Additionally, under the N2 atmosphere, a finer grain structure is observed, whereas the Ar atmosphere results in coarse and elongated grains [5]. However, in additively manufactured 17-4PH, the behaviour is different in recrystallization and precipitation due to the anisotropic microstructure. Therefore, microstructure homogenization are essential to obtain good mechanical properties for additively manufactured 17-4PH [6].

This research aims to contribute to understanding how the geometry and powder bed fusion manufacturing parameters affect the mechanical properties of 17-4PH stainless steel. This analysis aims to determine the mechanical properties, such as modulus and elastic limit, with different test geometries under the same parameters.

2. MATERIALS AND METHODS

2.1 Sample Fabrication

CONCEPTLASER M2 Cusing Multilaser machine at the Center for Engineering and Industrial Development (CIDESI) in Querétaro, Mexico was used for sample fabrication. The machine specifications are shown in Table-1.

Table-1. Machine specifications.

Fabrication dimensions (mm) (x, y, z)	250 x 250 x 280
Layer thickness (mm)	20 - 80
Production speed (cm³/h) (depending on the material/laser power)	2 - 35
Laser power (W):	2 x 200
Scanning speed (m/s)	Max. 4,5
Laser diameter (µm)	50 - 500
Operating conditions	15 - 35
Base plate material	316 SS
Base plate dimensions (mm)	245 x 245
Test temperature (°C):	23 - 25
Gas type	Argon Gas

The mechanical properties and defects generated in additively manufactured parts largely depend on the chemical composition of the material. It should be noted that the chemical composition of the material varies depending on the supplier. The supplier of the precipitation-hardened stainless-steel powder (17-4PH) is CONCEPTLASER, an additive company under GE, which has a chemical composition shown in Table-2.

Table-2. Chemical composition of 17-PH stainless steel [7].

Element	Indicative value (Weight in %)
C	0 - 0,07
Mn	0 - 1
P	0 - 0,04
S	0 - 0,03
Si	0 - 1
Cr	15 - 17,5
Ni	3 - 5
Cu	3 - 5
Nb + Ta	0,15 - 0.45
Fe	Balance

Samples were fabricated using the powder bed fusion technique with various parameters, but the most important ones were those inside the sample. The laser power used was 370 W, the laser speed was 800 mm/s, the hatch spacing was 0.12 mm, and the laser diameter was 135 µm. The different parameters that make up the sample can be observed in Figure-1.

Figure-1. Parameters of each specimen body.
Source: Author

Table-3 details the different parameters used in the manufacturing process. Parameter 5 was used for the base of the specimen; parameter 3 was the most important as it was used for the manufacturing of the body or interior, and the other three parameters were for the

surface. In addition, the manufacturing angle for specimens 1, 2, and 4 was 0°, while for specimens 3, 5, and 12, it was 45°. Figure-2 below shows the laser movement for each respective angle.

Table-3. Fabrication parameters.

Parameter	Power [W]	Scan Speed [mm/s]	Trace Spacing [mm]	Spot Size [µm]
5	200	1100	0,085	135
3	370	800	0,12	135
Purple	100	950	0,12	50
Red	200	1100	0,085	135
Black	100	350	0,12	50

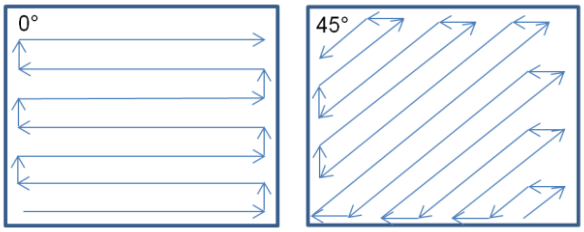

Figure-2. Shows the laser movement for each angle, respectively.

The dimensions of the specimens are shown in the Figurer-3; the six specimens´s fabrications have three different geometries; that is, 2 and 3 share the same 4 mm width and 4 mm radius geometry (Figure-3a), 5 and 1 have a width of 10 mm and a radius of 1 mm (Figure-3b), and finally, 4 and 12 are 7 mm wide and have a radius of 2.5 mm (Figure-3c). The E8 standard for tension test was followed.

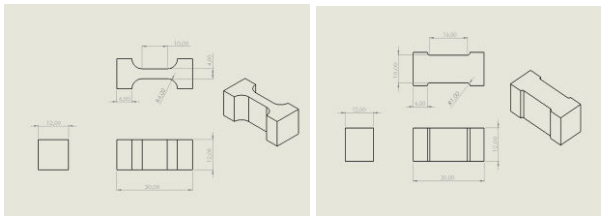

(a) (b)

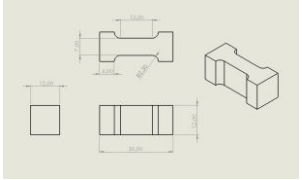

(c)

Figure-3. Dimension of the specimens a) 4 mm radius specimen, b) 1 mm radius specimen, c) 2.5 mm radius specimen. Source: Authors.

After fabrication, six pieces were obtained, as shown in Table-4.

Table-4. Fabricated specimens.

Specimen # 1	
Specimen # 2	
Specimen # 3	
Specimen # 4	
Specimen # 5	
Specimen # 12	

2.2 Tensile Test Procedure

First, the specimens fabricated by powder bed were cut to have several slices of approximately 1 mm thickness to perform the tensile tests. The diamond disc used for cutting the six specimens was a 12 x 0.4 x 12.7 mm Struers brand disc in an Accutom-100 cutter with a speed of 0,015 mm/s at 2500 rpm. The specimens were cut with the diamond disc, which took approximately 30 minutes per piece. In the end, two slices were obtained per probe, as seen in Figure-4; only the second smooth slice was used for the tensile test.

Figure-4. Thickness 1 mm probe cut. Source: Authors

After cutting the specimen, the width and thickness were manually measured three times with a digital calliper to obtain an average, and they were recorded in Table-5.

Table-5. Specimen´s dimensions.

	Width (mm)				Thickness (mm)			
	1	**2**	**3**	**Avar**	**1**	**2**	**3**	**Avar**
2	4,21	4,14	4,15	4,16	1,56	1,55	1,56	1,55
3	4,17	4,14	4,17	4,16	1,03	0,99	0,98	1,00
4	7,24	7,15	7,15	7,18	1,55	1,52	1,50	1,52
5	10,07	10,13	10,09	10,09	1,77	1,77	1,77	1,77
12	7,16	7,25	7,28	7,23	1,14	1,06	1,01	1,07
1	10,11	10,08	10,1	10,09	1,41	1,4	1,41	1,40

Furthermore, the area was obtained by multiplying the average width by the average thickness of each specimen, as shown in Table-6, as well as the calibrated length for the experimental tensile tests of each specimen (L_o). These measurements are used to calculate the strain of each specimen.

Table-6. Calculated area and L_o of the specimens.

Area (mm^2)		**Lo (mm)**
2	**6,486**	**15,35**
3	4,160	13,61
4	10,938	13,66
5	17,871	13,34
12	7,736	14,38
6	14,203	12,78

In the experimental tensile test, the midpoint of each specimen was first located to ensure that they were centered in the jaws. The piece was then mounted in the universal machine with a controlled environment, as observed in Figure-5, and the test was performed by applying load until the specimen fractured.

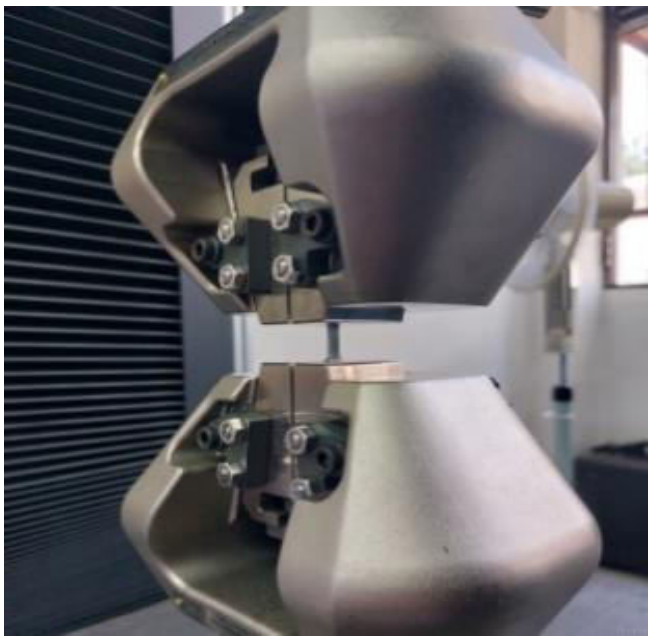

Figure-5. Tensile test of the specimens in the machine. Source: Authors

Data obtained from the experimental tensile test was used to calculate the stress using Equation 2:

$$\sigma = \frac{F}{A_o} \quad (2)$$

Where:
σ is the stress
F is the force
A_o is the cross-sectional area of the specimen and the strain is calculated using Equation 3:

$$\varepsilon = \frac{\Delta L}{l_o} \quad (3)$$

Where:
ε is the strain
ΔL is the difference in length
l_o is the calibrated length

The offset method was used to determine the yield strength. This method employs an offset of 0.2% from the slope according to the ASTM E8 standard; secant method was applied to obtain the elastic modulus,

3. RESULTS

An experimental tensile test was performed for each specimen, obtaining the following results

3.1 Specimen 1

For specimen 1 with a radius of 1 mm, total fracture occurred in 287,82 seconds (Figure-6), with a maximum strain of 0,3751 [mm/mm] and a maximum stress of 876,3 MPa. Figure 7 shows the Stress vs Strain plot for specimen 1.

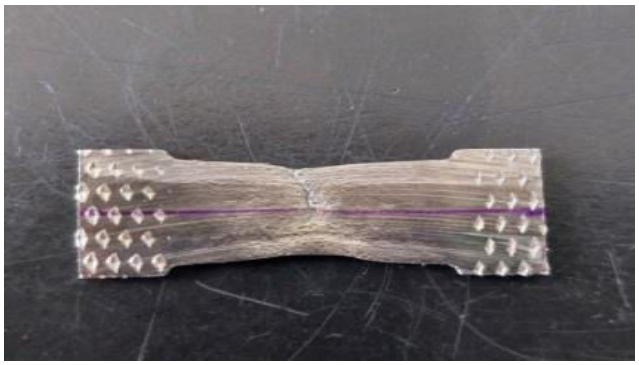

Figure-6. Failure for specimen 1 after tension test.
Source: Authors.

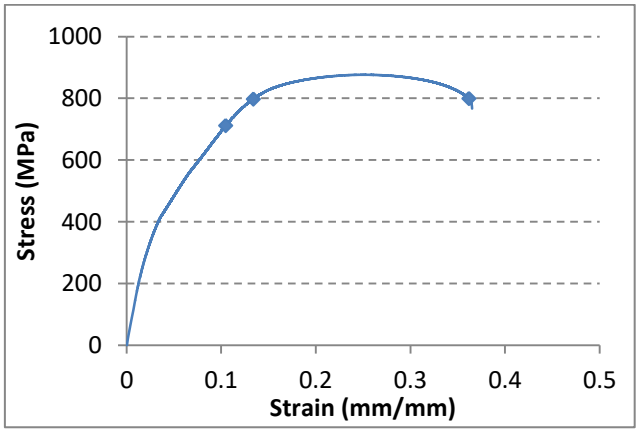

Figure-7. Stress Vs. Strain for specimen 1.

The mechanical properties determined from Figure-7 for specimen one is shown in Table-7 below.

Table-7. Mechanical properties for specimen 1.

Tensile strength	860,17	MPa
Young´s Modulus	16,70	GPa
Yield strength	276,76	MPa

3.2 Specimen 2

For specimen number two with a radius of 4 mm, the total rupture was obtained in 195,6 seconds (Figure-8), a maximum deformation of 0,212 (mm/mm) and a maximum stress of 865,209 MPa.

Figure-8. Failure for specimen 2 after tension test.
Source: Authors.

Figure-9 shows the Stress vs Strain plot for specimen number two, from which the mechanical properties of the additively manufactured material can be obtained.

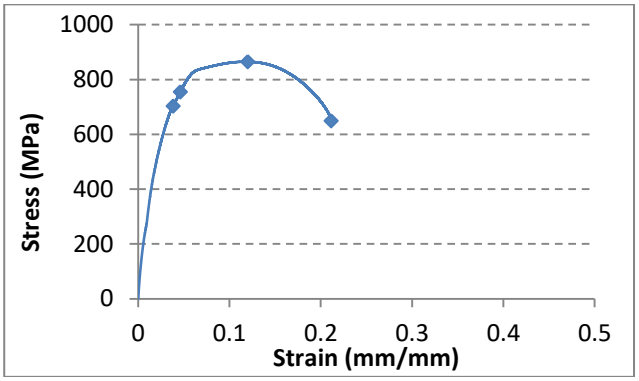

Figure-9. Stress Vs. Strain for specimen 2.

The mechanical properties extracted from the graph for specimen number two are shown in the following Table-8.

Table-8. Mechanical properties for specimen 2.

Tensile strength	863,38	MPa
Young´s Modulus	69,45	GPa
Yield strength	251,74	MPa

3.3 Specimen 3

For specimen number three, with a radius of 4 mm, the total rupture was obtained in 150,38 seconds (Figure-10), with a maximum deformation of 0,18389 (mm/mm) and a maximum stress of 823,089 MPa. Figure-11 shows stress vs deformation for specimen number three.

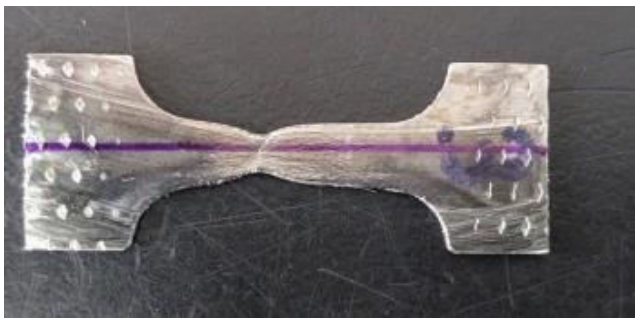

Figure-10. Failure for specimen 2 after tension test. Source: Authors.

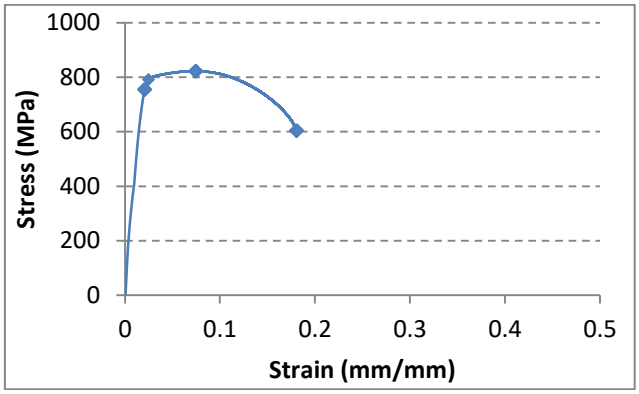

Figure 11. Stress Vs. Strain for specimen 3.

The mechanical properties extracted from the graph for specimen number three are shown in the following Table-9.

Table 9. Mechanical properties for specimen 3.

Tensile Strength	825,07	MPa
Young´s Modulus	61,12	GPa
Yield Strength	367,61	MPa

3.4 Specimen 4

For specimen number four, with a radius of 2.5 mm, the total rupture was obtained in 267,47 seconds (Figure-12), with a maximum deformation of 0,3261 (mm/mm) and a maximum stress of 862,977 MPa. Figure-12 shows stress vs deformation for the specimen.

Figure-12. Failure for specimen two after tension test. Source: Authors.

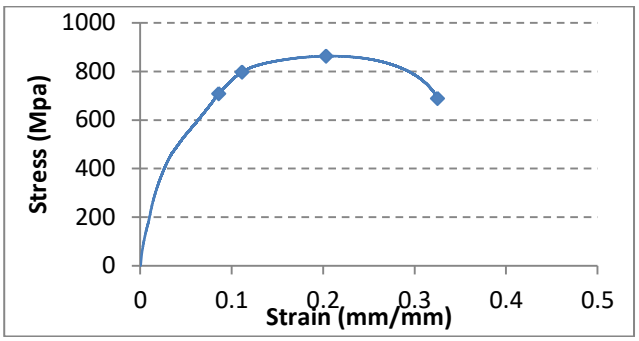

Figure-13. Stress Vs. Strain for specimen 4.

The mechanical properties extracted from the graph for specimen number four are shown in the following Table-10.

Table-10. Mechanical properties for specimen 4.

Tensile Strength	863,66	MPa
Young´s Modulus	35,58	GPa
Yield Strength	237,66	MPa

3.5 Specimen 5

For specimen number five with a radius of 1 mm, the total rupture was obtained in 354,12 seconds (Figure-14) with a maximum deformation of 0,4422 (mm/mm) and a maximum stress of 906,99 MPa. Figure-15 shows stress vs deformation for specimen number five.

Figure-14. Failure for specimen two after tension test. Source: Authors.

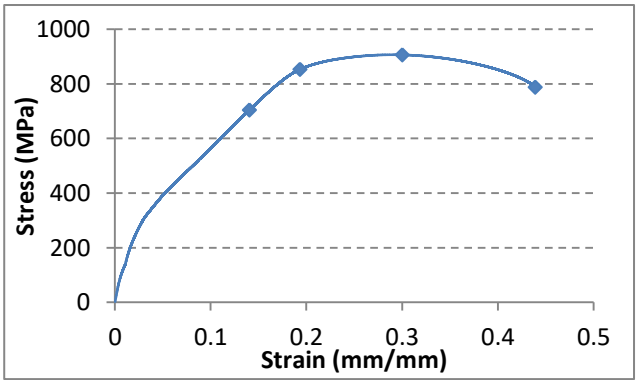

Figure-15. Stress Vs. Strain for specimen 5.

The mechanical properties extracted from the graph for specimen number five are shown in the following Table-11.

Table-11. Mechanical properties for specimen 5.

Tensile strength	1004,90	MPa
Young´s Modulus	259,05	GPa
Yield strength	872,43	MPa

3.6 Specimen 12

For specimen number twelve, with a radius of 2.4 mm. total rupture was obtained in 206,26 seconds (Figure-16), with a maximum deformation of 0,2388 (mm/mm) and a maximum stress of 809,24 MPa. Figure-17 shows stress vs deformation for specimen number twelve.

Figure 16. Failure for specimen 12 after tension test. Source: Authors.

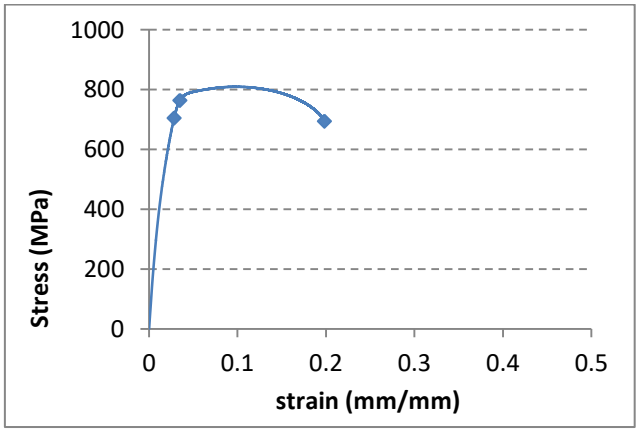

Figure-17. Stress Vs. Strain for specimen 12.

The mechanical properties extracted from the graph for specimen number twelve are shown in the following.

Table-12. Mechanical properties for specimen 12.

Tensile strength	816,88	MPa
Young´s Modulus	40,68	GPa
Yield strength	424,99	MPa

3.7 Mechanical Properties Comparison

As a result, three mechanical properties were obtained for each specimen. Figure-18 shows the ultimate tensile strength of the six tension tests. The tensile strength's highest value is 1004, 9 MPa from specimen 5, and, in contrast, the lowest of 816, 88 MPa from specimen 12.

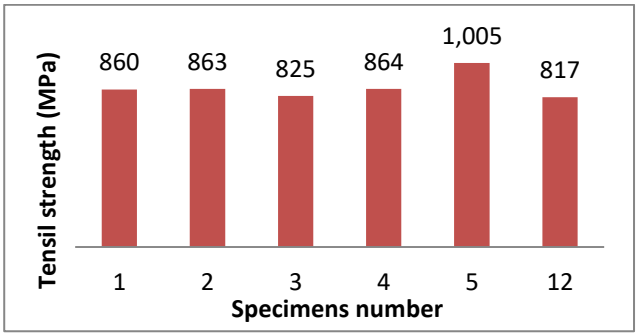

Figure-18. Comparison of tensile strength specimen´s.

Figure-19 shows the yield strength values obtained for each specimen. The highest yield strength was obtained from specimen 5, with a value of 872, 43 MPa, while the lowest value was obtained from specimen 12 with 748,36 MPa.

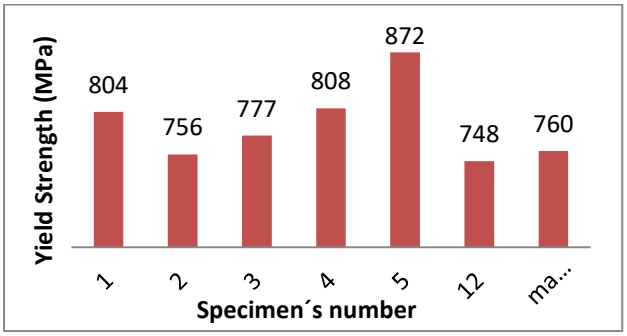

Figure 19. Comparison of yield strength specimen´s.

Specimen 5 also exhibited the highest modulus of elasticity, with a value of 259, 05 GPa, while specimen 1 had the lowest value, with 16, 7 GPa as shown in Figure-20.

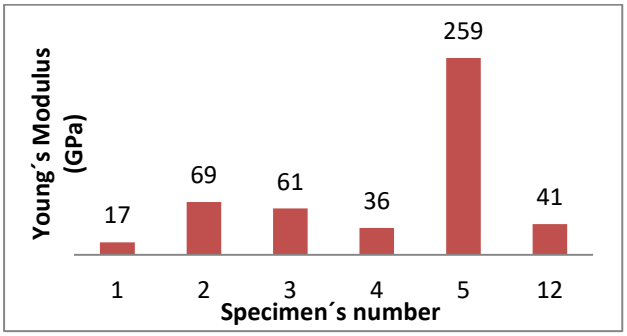

Figure-20. Comparison of Young´s Modulus specimen.

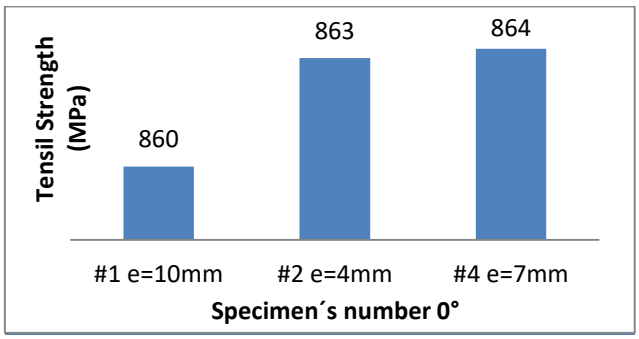

Figure-21. Comparison of tensile strength for specimens impressed to 0°.

Figure-22 shows the yield strength of the three specimens fabricated at a 0° angle. The highest value was recorded for specimen 4 with 808, 45 MPa, while the lowest was for specimen 2 with 755,89 MPa.

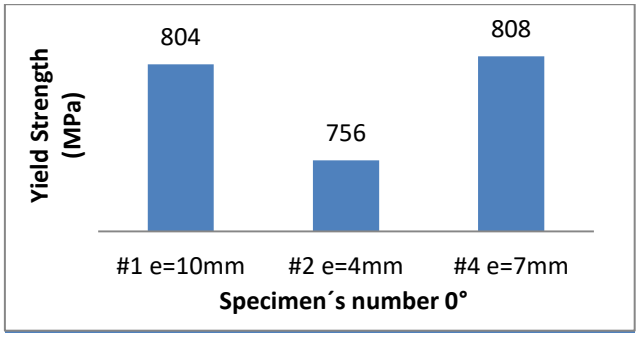

Figure-22. Comparison of yield strength for specimens impressed to 0°.

The modulus of elasticity of the three specimens fabricated at a 0° angle can be seen in Figure-23. The highest value was recorded for specimen 2 with 69,45 GPa, while the lowest was for specimen 1 with 16,7 GPa.

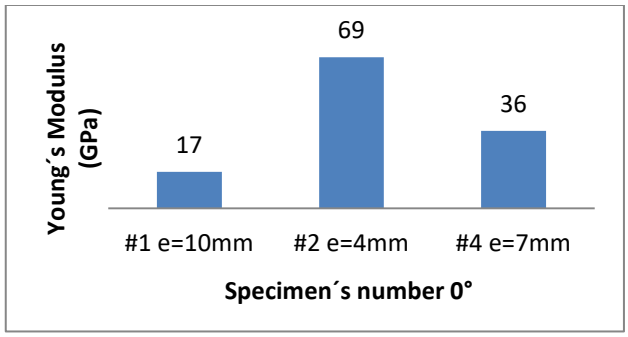

Figure-23. Comparison of Young´s Modulus for specimens impressed at 0°.

Figure-24 displays the ultimate stress for the three specimens fabricated at a 45° angle. The highest value was recorded for specimen 5 with 1004,9 MPa, while the lowest was for specimen 12 with 816,88 MPa.

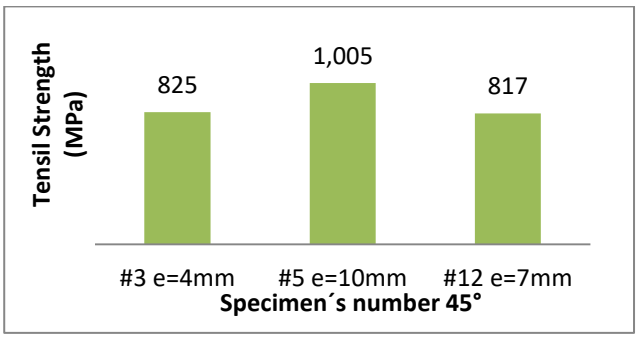

Figure-24. Comparison of tensile strength for specimens impressed at 45°.

Figure-25 shows the yield strength of the three specimens fabricated at a 45° angle. The highest value was recorded for specimen 5, 872, b43 MPa, while the lowest was for specimen 12, 748, 36 MPa.

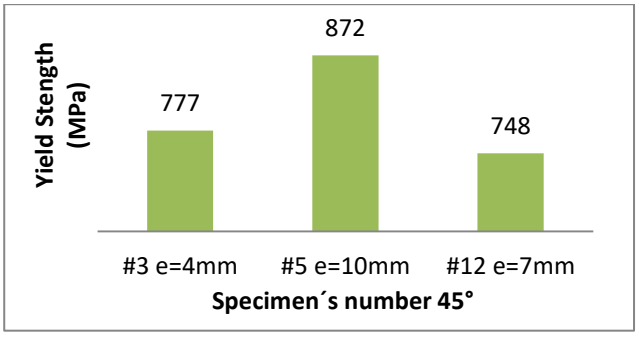

Figure-25. Comparison of yield strength for specimens impressed to 45°.

The modulus of elasticity of the three specimens fabricated at a 45° angle can be seen in Figure-26. The highest value was recorded for specimen 5, with 259, 05 GPa, while the lowest was for specimen 12, with 40,676 GPa.

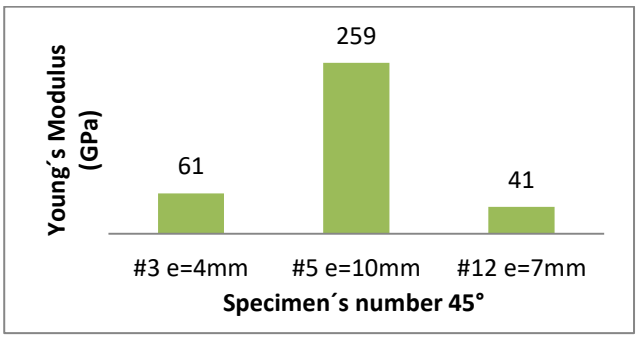

Figure-26. Comparison of Young´s Modulus for specimens impressed at 45°.

4. DISCUSSIONS

The mechanical properties such as modulus of elasticity, yield strength, and ultimate strength obtained by experimental tests on specimens manufactured by powder bed fusion were not the best or most ideal to meet the

requirements of any industrial application. The modulus of elasticity is relatively small, mainly due to process parameters and residual stresses generated during the process. Additionally, the low modulus of elasticity is attributed to pores between layers in additive manufacturing, which reduces the material's elastic capacity.

Furthermore, the fabrication angle also affects the mechanical properties. When specimens are fabricated at a 0° angle, the layers are joined horizontally, and tensile forces are applied vertically along the Y-coordinate during testing, causing layer separation. The same is true for specimens fabricated at a 45° angle, but the forces applied are less, resulting in less layer separation than at 0°. The results are mainly due to process parameters and residual stresses generated during the process.

The tensile behaviour of the material in its manufactured condition is highly dependent on the powder's chemical composition. The complex chemical composition may include more martensite or ferrite and high austenite levels. Murr *et al.* [8] research showed that the additive manufacturing of 17-4PH stainless steel powder with argon gas (Ar) resulted in an entirely martensitic microstructure. However, recent studies with the same Ar characteristics have formed both martensite and austenite [9]. The difference in microstructure behaviour is due to variations in chemical composition and fabrication conditions, which include machine parameters and part geometry, resulting in different thermal histories during fabrication. In the stress-strain graph of the experimental tension tests, the continuous line has abnormal behaviour, i.e. it has two slopes in the elastic zone.

Additionally, the plot behaviour is still influenced by changes in chemical composition, residual stresses, and heterogeneous segregation throughout the sample due to thermal cycles and cooling rates.

5. CONCLUSIONS

The mechanical properties obtained from the experimental tensile tests were not optimal, the fabrication angle of the specimens have the most significant impact on the process. Thus, the specimens' ultimate strength, yield strength, and modulus of elasticity were meagre.

The stress-strain experimental graphs have an unusual behaviour in the elastic region due to the stainless steel's martensitic transformation caused by applying stresses in the tensile test, increasing the modulus and elastic limit of the material.

It can be concluded that for a fabrication angle of 90°, the mechanical properties will be better than for other angles, such as 0° and 45°, because the applied forces will be in the same direction as the fibres, unlike other angles where they are perpendicular, leading to separation between layers and resulting in lower mechanical properties.

ACKNOWLEDGMENTS

The Center for Engineering and Industrial Development (CIDESI) and the CONACYT consortium for Additive Manufacturing (CONMAD) are acknowledged for allowing the experimental tests, and the faculty members of the Mechanical Engineering program at the University of Pamplona for their valuable support and knowledge provided.

REFERENCES

[1] D., Ntamo *et al.* 2022. Industry 4, 0 in Action: Digitalisation of a Continuous Process Manufacturing for Formulated Products. Digit, Chem, Eng,, 3(February): 100025, doi: 10,1016/j,dche,2022,100025.

[2] R., Pinto and G., Gonçalves. 2022. Application of Artificial Immune Systems in Advanced Manufacturing. Array, 15(October 2021): 100238, 2022, doi: 10,1016/j,array,2022,100238.

[3] J., De Ciurana, L., Serenó and È. Vallès. 2013. Selecting process parameters in RepRap additive manufacturing system for PLA scaffolds manufacture. Procedia CIRP, 5: 152-157, doi: 10,1016/J,PROCIR,2013,01,031.

[4] Z., Yan *et al.* 2018. Review on thermal analysis in laser-based additive manufacturing. Opt, Laser Technol, 106: 427-441, doi: 10, 1016/j,optlastec,2018,04,034.

[5] S., Sabooni *et al*. 2021. Laser powder bed fusion of 17-4 PH stainless steel: A comparative study on the effect of heat treatment on the microstructure evolution and mechanical properties. Addit, Manuf, 46(June): 102176, doi: 10,1016/j,addma,2021,102176.

[6] K., Li *et al*. 2022. Homogenization timing effect on microstructure and precipitation strengthening of 17-4PH stainless steel fabricated by laser powder bed fusion. Addit, Manuf, 52(November 2021): 102672, doi: 10, 1016/j,addma,2022,102672.

[7] C., Composition. Fe 55,847.

[8] L. E., Murr *et al*. Microstructures and properties of 17-4 PH H, Eskandari, H, R, Lashgari, L, Ye, M, Eizadjou, and H, Wang. 2022. Microstructural characterization and mechanical properties of additively manufactured 17-4PH stainless steel. Mater, Today Commun,, 30 (December 2021), doi: 10,1016/j,mtcomm,2021,103075.